First Demonstration of Ocular Refractive Change Using Blue-IRIS in Live Cats

Daniel E. Savage,[1,2] Daniel R. Brooks,[1] Margaret DeMagistris,[3] Lisen Xu,[*,1] Scott MacRae,[2,3] Jonathan D. Ellis,[1,4] Wayne H. Knox,[1,2] and Krystel R. Huxlin[2,3]

[1]The Institute of Optics, University of Rochester, Rochester, New York, United States
[2]Center for Visual Science, University of Rochester, Rochester, New York, United States
[3]Flaum Eye Institute, University of Rochester, Rochester, New York, United States
[4]Department of Mechanical Engineering, University of Rochester, Rochester, New York, United States

Correspondence: Krystel R. Huxlin, University of Rochester Eye Institute, 601 Elmwood Avenue, Box 314, Rochester, NY 14642,USA; huxlin@cvs.rochester.edu

DES and DRB are equal first authors.

JDE, WHK, and KRH are equal senior authors.

Current affiliation: *Optikos Corporation, Wakefield, Massachusetts, United States.

Submitted: March 17, 2014
Accepted: June 10, 2014

Citation: Savage DE, Brooks DR, DeMagistris M, et al. First demonstration of ocular refractive change using blue-IRIS in live cats. *Invest Ophthalmol Vis Sci*. 2014;55:4603–4612. DOI:10.1167/iovs.14-14373

Purpose. To determine the efficacy of intratissue refractive index shaping (IRIS) using 400-nm femtosecond laser pulses (blue light) for writing refractive structures directly into live cat corneas in vivo, and to assess the longevity of these structures in the eyes of living cats.

Methods. Four eyes from two adult cats underwent Blue-IRIS. Light at 400 nm with 100-femtosecond (fs) pulses were tightly focused into the corneal stroma of each eye at an 80-MHz repetition rate. These pulses locally increased the refractive index of the corneal stroma via an endogenous, two-photon absorption process and were used to inscribe three-layered, gradient index patterns into the cat corneas. The optical effects of the patterns were then tracked using optical coherence tomography (OCT) and Shack-Hartmann wavefront sensing.

Results. Blue-IRIS patterns locally changed ocular cylinder by -1.4 ± 0.3 diopters (D), defocus by -2.0 ± 0.5 D, and higher-order root mean square (HORMS) by 0.31 ± 0.04 μm at 1 month post-IRIS, without significant changes in corneal thickness or curvature. Refractive changes were maintained for the duration they were tracked, 12 months post-IRIS in one eye, and just more than 3 months in the remaining three eyes.

Conclusions. Blue-IRIS can be used to inscribe refractive structures into live cat cornea in vivo that are stable for at least 12 months, and are not associated with significant alterations in corneal thicknesses or radii of curvature. This result is a critical step toward establishing Blue-IRIS as a promising technique for noninvasive vision correction.

Keywords: femtosecond, refractive index, IRIS

Laser in situ keratomileusis (LASIK), photorefractive keratectomy (PRK), and all the variants of laser refractive surgery that have followed,[1] are similar in that they correct visual refractive errors by ablating corneal tissue, usually the corneal stroma. Laser photo-ablation of the stromal bed is typically accomplished via a single-photon absorption mechanism at 193 nm.[2] It is used to change the shape of the cornea's anterior surface, thus altering its refractive properties and optical power.

Instead of changing the surface curvature, changing the refractive index (RI) is an alternative means of modifying the focusing properties of a refractive optical element, such as the cornea. In 2010, building on previous work with infrared pulses,[3–9] we first reported writing RI patterns in corneal tissue using 400-nm femtosecond (fs) pulsed laser light.[10] This new process, termed Blue-Intratissue Refractive Index Shaping (Blue-IRIS), achieved RI changes as high as +0.037 at speeds of 5 mm/s.[10,11] The magnitude of the RI change was ascertained by measuring the diffraction efficiencies of Blue-IRIS–inscribed phase gratings.[3,5] Although the exact mechanism of RI change in cornea is not yet fully understood, some of its features seemed consistent with the low-density electron plasma model for femtosecond laser-material interactions set forth by Vogel and colleagues.[12–14]

However, the Blue-IRIS writing geometry used in our original work did not create refractive structures that could change refractive power. In the present report, we used Blue-IRIS to write 2.5×2.5-mm^2 refractive, lateral gradient index (GRIN) microlenses into the corneas of living cats in vivo. Our primary goal was to induce a refractive change of at least −1 diopter (D) cylinder into living corneal tissue. We then ascertained the longevity of such a pattern in the living eye, and determined whether the writing process induced any significant changes in the thickness or curvature of different corneal layers. Demonstrating the ability of Blue-IRIS to induce stable, refractive changes in the eye is an essential first step toward establishing its efficacy and its potential as a new approach for refractive correction.

Materials and Methods

Experimental Setup

The femtosecond laser micromachining system developed for the present experiments (Fig. 1) used a mode-locked femtosecond Ti:Sapphire oscillator (Vitesse; Coherent Corporation, Santa Clara, CA, USA). This laser emitted 800-nm, 100-fs pulses at an 80-MHz repetition rate. The average output power at 800 nm was up to 1 W. The 800-nm beam was frequency doubled to 400 nm by using a second harmonic generator to produce up to approximately 250 mW of 400-nm femtosecond pulses. The

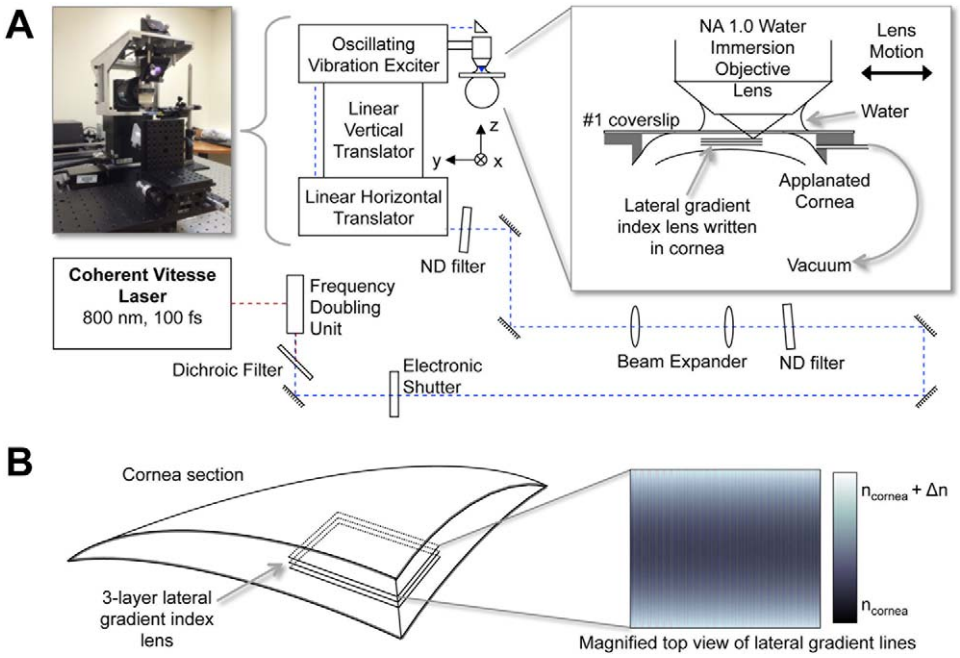

Figure 1. Blue-IRIS experimental setup. (**A**) Pulses of 800 nm, 100 fs, from a Ti:Sapphire oscillator are frequency doubled to produce 400-nm, 100-fs pulses. These pulses are then attenuated and delivered through a 1.0-NA water immersion objective into the cornea of a live cat. The average power in the focal region of the objective is 60 mW. The cornea is applanated using a #1 microscope slide mounted on a custom-made suction ring. The focal region of the objective is scanned through the cornea using a three-axis delivery system to inscribe the Blue-IRIS pattern in the cornea. (**B**) A schematic of a corneal segment containing an inscribed, midstromal (280 to 300 μm below the epithelium), three-layer Blue-IRIS pattern. The inset shows a top-view representation of a single Blue-IRIS gradient index layer used to induce a negative change in cylinder with the largest positive refractive index changes at the top and the bottom (*lightest shading*), and the smallest RI changes in the middle of the structure (*darkest shading*). The resulting RI-change structure is intended to exert a phase-shifting effect on the incident light, with phase retardation increasing with increasing RI.

400-nm blue laser light was passed through an electronic shutter (Uniblitz; Vincent Associates, Rochester, NY, USA), then a coarsely adjustable, metallic variable neutral density (ND) filter, before being expanded to approximately 17 mm full width at half maximum to fill the entrance pupil of the micromachining objective. After expansion, the beam was passed through a finely adjustable metallic variable ND filter. It was then guided through a three-axis beam delivery system. Finally, the beam was focused into the stroma of the cat cornea via a high-numerical aperture (NA = 1.0), water-immersion microscope objective (W Plan-Apochromat, ×20; Carl Zeiss, Jena, Germany). The cornea was applanated with a thin (170 μm) glass plate. The power in the focal region of the objective was attenuated to 60 ± 1 mW, corresponding to pulse energies of approximately 0.8 nJ.

The three-axis beam delivery system consisted of a commercial vibration exciter (Measurement Exciter Type 4810; Brüel & Kjær, Nærum, Denmark) mounted on a vertical-translation stage (GTS30V; Newport Corporation, Irvine, CA, USA) that was mounted on a single-axis linear translator (GTS70; Newport Corporation). This three-axis configuration allowed the live cat cornea to remain stationary while the delivery system rapidly scanned the focal region of the 400-nm beam. While a single GRIN layer was being written in a sample, the linear horizontal stage was translated at 8 μm/s in the *x*-direction; the vertical translation stage was kept stationary, and the vibration exciter oscillated in the ± *y*-direction at 4 Hz (Fig. 1A). This generated a roughly sinusoidal pattern of increased RI with 1-μm center-spaced lines. Because the line widths were approximately 1 μm, this dense pattern of lines formed a nearly continuous gradient index, phase-retarding structure, thereby functioning as a refracting lens. The vibration exciter was driven with a custom waveform to achieve the desired RI pattern for each layer and an electronically controlled shutter was synchronized to the vibration exciter to block the laser beam at the vibration exciter turnaround points where the scanning velocity temporarily goes to zero.

Experimental Procedures

Both eyes from two young adult (~1.0- to 1.5-year-old), domestic short hair cats (*Felis cattus*) were used for the present experiments. All animal procedures were conducted according to the guidelines of the ARVO Statement for the Use of Animals in Ophthalmic and Vision Research, and the National Institutes of Health Guide for the Care and Use of Laboratory Animals. The protocol was approved by the University of Rochester Committee on Animal Research (UCAR assurance number: A-3292-01).

We first performed wavefront sensing and optical coherence tomography (OCT) imaging in each eye using custom-built instruments to collect baseline measures of ocular aberrations, corneal thickness, and corneal curvature, as previously described.[15,16] An approximately 2.5 × 2.5-mm^2, −1 D cylinder Blue-IRIS lens was then inscribed slightly eccentric relative to the pupillary center of each eye. Ocular aberrations, corneal thickness, and corneal curvatures were re-measured at semiregular time points for up to 12 months post-IRIS at the time of writing of this report.

Blue-IRIS Procedures in Living Cats

Intratissue Refractive Index Shaping procedures were executed under topical (proparacaine 0.5%; Falcon) and surgical anesthesia (ketamine, 5 mg·kg^{-1}, dexmedetomidine hydrochlo-

ride 0.04 mg·kg^{-1}). First, each cornea was flat-applanated using a custom-built suction ring that fit inside the feline palpebral aperture. This device consisted of a polycarbonate ring with an inner opening 6 mm in diameter and a #1 (170-μm-thick), round, glass, microscope cover-slip (VWR, Radnor, PA, USA) sealed to its top surface (Fig. 1A). A flat-edged needle inserted into a small hole in the side of the ring and connected to a spring-loaded syringe allowed us to apply vacuum suction to the inside of the ring. Once applanated, the cornea was centered to the water-immersion focusing objective used to deliver the blue laser light. Three successive, nominally identical, lateral GRIN layers were inscribed with an intended vertical spacing of 10 μm, to increase the total refractive power of the written structure, by using the Vitesse femtosecond laser system described above (Fig. 1A). The layers were written in the corneal midstroma at intended depths of 300 μm, 290 μm, and 280 μm below the epithelial surface, respectively; the mean pre-IRIS central thickness of the cat corneas was found to be 588 ± 34 μm, which is in good agreement with published values for normal cats.[17] Each layer was a square shape, with sides 2.5 × 2.5 mm^2, and was written nominally parallel to the applanator.

Wavefront Sensing and Analysis in Awake, Fixating Cats

Wavefront measurements were collected before, and at semi-regular time points after Blue-IRIS treatment by using a custom-built, Shack-Hartmann wavefront sensor, as previously described.[16,18–22] The wavefronts were measured over the full pupil; however, the aberrations were analyzed only over an eccentric, 3-mm-diameter area centered on the region in which the Blue-IRIS pattern was inscribed. This allowed us to quantify changes in ocular wavefront aberrations induced by Blue-IRIS. In brief, both cats were behaviorally trained for several months, until they were able to precisely fixate on single spots of light presented on a computer monitor. The wavefront sensor was then aligned to the visual axis of one eye with a pupil camera, while the other eye continued to fixate a spot of light presented on a dark computer monitor. Several hundred video frames of each eye's spot array patterns were collected at each time-point during fixation intervals. At least 12 of these video frames were analyzed per eye at every time-point, and wavefront errors were calculated using a 2nd-order through 10th-order Zernike polynomial expansion according to published standards for reporting aberration data of the eye.[23]

Wavefront sensing was performed as soon as possible (1 to 2 days) after Blue-IRIS. The exact timing of this early, post–Blue-IRIS imaging session depended on how well the animals recovered from anesthesia, and thus, how soon they were able to undergo wavefront sensing in the awake-fixating state. For calculation of baseline wavefront aberrations, wavefront sensor spot patterns collected before Blue-IRIS were analyzed with the 3-mm-diameter analysis region shifted according to the mean post-IRIS offset relative to the pupil center. This allowed us to compare approximately the same region of cornea before and after IRIS.

In addition to quantifying lower-order and higher-order aberrations, we also computed the following at each time-point: lower-order root mean square (LORMS), higher-order RMS (HORMS), and the optical power induced by Blue-IRIS in diopters. Because the measured wavefronts were decomposed into a variance-normalized Zernike base, the RMS values were calculated from the Zernike coefficients via equation 1,[24]

$$RMS = \sqrt{\sum_j (C_j)^2}, \quad (1)$$

where C_j is the jth Zernike coefficient. LORMS was calculated using Equation 1 for $j = 3$ to 5; Similarly, HORMS was calculated for $j = 6$ to 65. The defocus and cylinder powers induced by Blue-IRIS were calculated from the second-order Zernike coefficients via Equation 2,

$$DEF = \frac{4\sqrt{3}C_4}{r^2}$$

$$CYL = -\frac{4\sqrt{6}\sqrt{(C_3)^2 + (C_5)^2}}{r^2}$$

$$\phi = \frac{1}{2}\tan^{-1}\left(\frac{C_3}{C_5}\right), \quad (2)$$

where these quantities are equivalent to sphero-cylindrical wavefront refractions except of opposite sign from the traditional formulae. This is because in the present study we were interested in the second-order optical power of the wavefront, not the spectacle correction.[24,25] In Equation 2, r is the pupil radius (1.5 mm in our case), *DEF* is the paraxial wavefront defocus, *CYL* is the paraxial wavefront cylinder, and ϕ is the angle of the cylinder axis.[2] In all applicable cases, values were expressed in terms of magnitude change relative to preoperative values, allowing us to compensate for differences in baseline between eyes.

Optical Coherence Tomography

A custom-built, anterior segment OCT was used to image feline corneas before and after Blue-IRIS to obtain thickness measurements of the epithelial and stromal layers of the cornea and corneal curvatures, as previously described.[16,26–31] Cats were anesthetized as detailed above for Blue-IRIS. Lubricating gel (GenTeal; Novartis, Basel, Switzerland) was applied to the ocular surface, the head was stabilized, and the OCT was centered on the pupil. Videos of the central 10 mm of each cornea were collected at 8 frames per second. At least 10 images were extracted at each time-point to compute the thickness and radius of curvature.

For thickness measurements, custom software was used to obtain a normalized intensity profile across a rectangular area 105 μm wide, spanning the entire thickness of the cornea, 1 mm nasal (to avoid the specular reflection) to the middle of each image. The thickness of the epithelium and stroma were estimated by measuring the difference between relevant intensity peaks in each profile, as previously described.[31,32]

Custom software also was used to determine curvatures from OCT images.[16] Specifically, the curvatures of the tear film–epithelial interface, epithelial-stromal interface, and the stromal-endothelial interface were calculated via a custom-edge detection algorithm over a 6-mm central anterior corneal region and a 5-mm posterior corneal region.

Results

General Observations

Immediately after Blue-IRIS, microbubbles appeared across the inscribed patterns, but they dissipated within several minutes, rendering the patterns nearly invisible and difficult, if not impossible, to visually locate from that point onward (Fig. 2A). Once recovered from general anesthesia, the cats did not exhibit any signs of ocular discomfort, as evidenced by squinting, excessive tearing, blinking, or abnormal behavior.

Investigative Ophthalmology & Visual Science

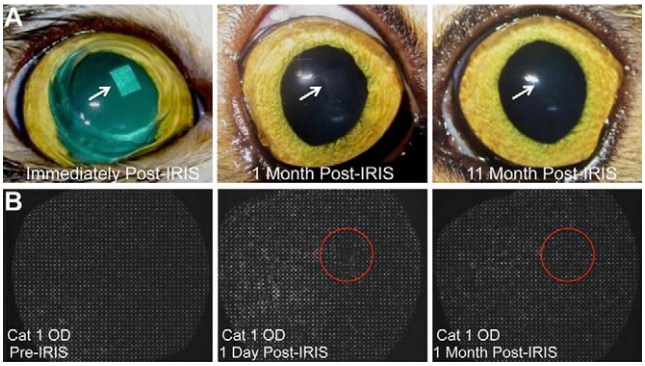

FIGURE 2. Photographs of Blue-IRIS patterns inscribed in live cats in vivo, and wavefront sensor spot arrays. (**A**) Representative Blue-IRIS patterns are shown. The inscribed patterns are initially visible, presumably due to micro-bubble formation. However, the bubbles dissipate within minutes, and the pattern becomes difficult, if not impossible, to visualize with the naked eye. (**B**) Spot array patterns collected by the Shack-Hartmann wavefront sensor pre-IRIS, 1 day post-IRIS, and 1 month post-IRIS in the same cat eye (Cat 1 OD). The *red circles* denote the approximate location of the IRIS pattern on each image.

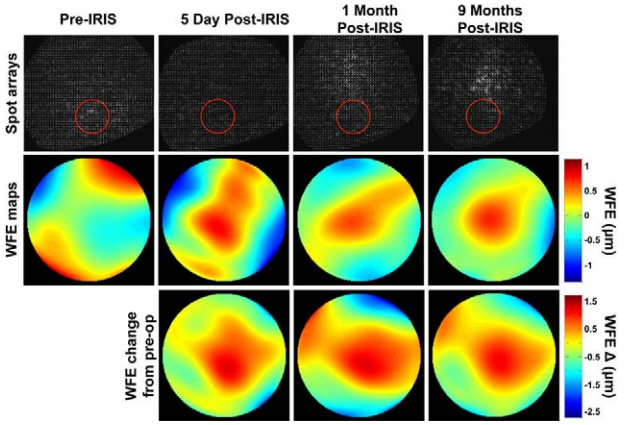

FIGURE 3. Representative wavefront spot arrays, raw wavefront error (WFE) maps, and wavefront error change maps relative to the pre-IRIS state from Cat 1 OS. Images of spot array patterns collected pre-IRIS as well as 5 days, 1 month, and 9 months post-IRIS in the same eye. Each reconstructed WFE map below the spot array patterns is the average of at least 14 wavefronts from the same time-point over a 3-mm-diameter analysis region centered on the nominal location of the IRIS pattern (*red circles* in spot array patterns above each WFE map). The change from pre-IRIS WFE maps are generated by subtracting the average pre-IRIS wavefront from the average wavefront at each time-point of interest post-IRIS. The inscribed Blue-IRIS pattern contributes the characteristic sphero-cylindrical shape present in all of the change from pre-IRIS wavefront maps, and which disappears whenever the analysis aperture is moved off the IRIS pattern area.

Effect of Blue-IRIS on Wavefront Aberrations

All of the cat eyes used in the present study had relatively low astigmatism and defocus, with no unusual visual defects, and with aberration distributions that were consistent with previously reported values for normal cat eyes.[15] This was also the case over the small, slightly off-center, analysis area (Figs. 3, 4; Table 1). The average total RMS ± SEM for that area ($n = 4$; excludes $j = 1$, 2) pre-IRIS was 0.36 ± 0.05 μm. LORMS averaged 0.27 ± 0.05 μm, and there were relatively few higher-order aberrations in these four eyes (Fig. 4B), with the HORMS averaging 0.24 ± 0.04 μm.

In terms of lower-order aberrations, Blue-IRIS changed both astigmatism and defocus. The amount of each astigmatism term induced by the procedure varied in each eye, largely because we cannot yet control the positioning and orientation of the square IRIS patterns relative to the pupil center. Nevertheless, IRIS generated an amount equal to or greater than the intended amount of cylinder change in each cat eye relative to the pre-IRIS state (Figs. 3, 5), which was stable for the duration it was tracked, up to 12 months at the time of this report in Cat 1 OS (Figs. 3, 5A) and 3 months in the remaining three eyes (Figs. 5B, 5C). The average cylinder power for each time-point per cat was calculated over the 3-mm-diameter analysis region using Equation 2 from difference relative to pre-IRIS data to remove baseline aberrations (Table 2). Across cats, this represented a mean ± SEM cylinder change of −1.4 ± 0.3 D. At the 12-month time-point, the greatest length of time examined at the time of this report, the mean ± SD cylinder change was found to be −1.9 ± 0.3 D for Cat 1 OS.

An unexpected finding was that Blue-IRIS also induced a large defocus change in the analysis region of each eye, relative to baseline (Fig. 6; Table 2). Across the four eyes, this represented a −2.0 ± 0.5 D (mean ± SEM) change relative to baseline levels.

Finally, average HORMS also increased slightly in the analysis region of all eyes post-IRIS (Fig. 7; Table 2). The HORMS peaked in the initial 1 to 3 days post-IRIS, and then declined to a relatively stable value. The mean ± SEM HORMS change across the four eyes was 0.31 ± 0.04 μm over the 3-mm-diameter analysis region. The increase in HORMS appeared predominately driven by spherical aberration ($j = 12$). At 1 month post-IRIS, the mean ± SEM ($n = 4$) spherical aberration coefficient was 0.09 ± 0.05 μm. The proportion of the higher-order variance occupied by spherical aberration was approximately 53%. In contrast, the spherical aberration coefficient at baseline was 0.004 ± 0.020 μm, which corresponded to only approximately 0.2% of the higher-order variance. None of the other higher-order variances experienced such a dramatic shift, suggesting that spherical aberration accounts for much of the increase in HORMS 1 month post-IRIS. The change in spherical aberration was found to be relatively stable for the duration of the study.

Effect of Blue-IRIS on Central Corneal Thickness and Curvature

Neither central corneal thicknesses nor any of the curvatures measured changed significantly after IRIS (Fig. 8; Table 3). Paired, two-tailed Student's *t*-tests revealed no statistically significant difference between the pre- and post-IRIS epithelium thickness values, or the pre- and post-IRIS stroma thickness values. Table 3 also shows the mean radius of curvatures in each of the four eyes for the tear film–epithelium interface, the epithelium-stroma interface, and the stroma-endothelium interface at both the pre-IRIS and 1 month post-IRIS time-points. None of these radii of curvature were found to have significantly changed using paired, two-tailed Student's *t*-tests.

Discussion

Blue-IRIS Induces Cylinder Change in Living Eyes

In this study, Blue-IRIS refractive structures were inscribed into the stromal layer of living cat eyes for the first time. We implemented a three-layered, lateral GRIN lens design intended to change cylinder by approximately −1 D (verified in hydrogels[33]). These animals were behaviorally trained to allow reliable measurements of ocular wavefront aberrations.[15] By

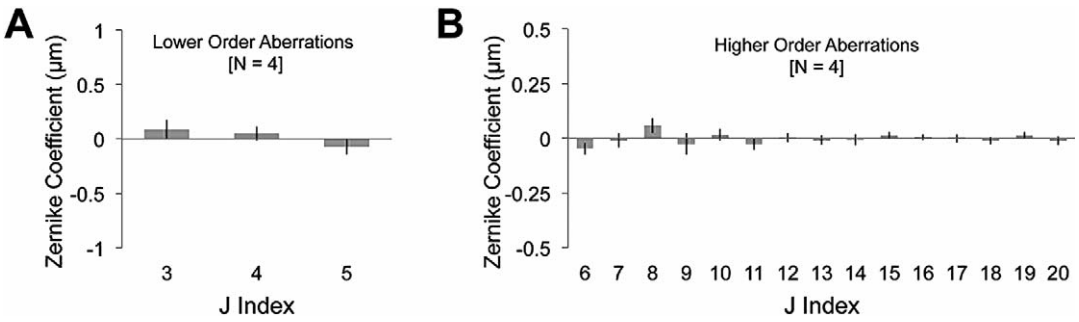

Figure 4. Magnitude of baseline (pre-IRIS) Zernike terms. (**A**) Plots of the magnitude of lower-order ($j = 3$–5) Zernike coefficients averaged across all four eyes in the study. (**B**) Plots of the magnitude of higher-order ($j = 6$–20) Zernike coefficients averaged across all four eyes in the study. In all cases, the data were collected over a 3-mm-diameter, circular region of the cat cornea that approximates the region over which the IRIS pattern would be inscribed. *Error bars* represent SEM.

comparing baseline and post-IRIS wavefront measures, we confirmed a mean induction across four eyes of approximately −1.4 ± 0.3 D in cylinder over the IRIS-inscribed areas of cornea. We were able to demonstrate stability of the refractive change over the entire period tracked: 3 months in three eyes and 12 months in one eye. However, our results also clearly demonstrated the need for additional refinement before we can generate precise optical outcomes.

Blue-IRIS Shows the Potential to Produce Deterministic Refractive Corrections

Indeed, with further refinements, Blue-IRIS could become more accurate, and ultimately create reproducible and reliable (i.e., deterministic) refractive corrections in the eye. Such refinements should include better control over the applanation, laser intensity, and scan speed control, as well as writing patterns over larger areas, better metrology, and so forth. Producing deterministic refractive corrections will also require a fuller understanding of potential biomechanical changes to the shape of the cornea.

To demonstrate a deterministic, induced cylinder change, the axis orientation of the cylinder also must be considered. With the current experimental apparatus, the angle of the cylinder, ø, could not be rigorously controlled or measured. Future work will develop a methodology for accurately and precisely relating the axis of the measured cylinder to the written orientation of the inscribed pattern.

Blue-IRIS Induced an Unintended Change in Defocus and Spherical Aberration

In addition to the induced cylinder power, a significant amount of negative (hyperopic) defocus and positive spherical aberration were also induced over the Blue-IRIS region in all four eyes. This unexpected result could have several causes. First, the defocus could have been exaggerated by the measurement method. The Blue-IRIS structures inscribed were approximately 2.5 × 2.5 mm^2 which underfill the 3-mm circular measurement aperture used by the wavefront sensor. It is thus possible that a portion of the actual cylinder power induced in the cornea was decomposed as defocus, due to the relatively low spatial frequency Zernike expansion over the underfilled measurement aperture. Our current Blue-IRIS experimental apparatus is being redesigned and rebuilt to allow for the writing of larger Blue-IRIS structures over at least a 6-mm-diameter area.

It is also possible that the induced defocus was caused by the lengthy applanation time currently required to perform Blue-IRIS. Although it only takes approximately 5 minutes to write a single 2.5 × 2.5-mm^2 GRIN layer into the cornea, aligning the cat eye to the beam delivery system increased the

Table 1. Baseline Second-Order Zernike Coefficients ($j = 3$–5), HORMS, Refractive Power, and Structural Parameters for Each Eye Pre-IRIS

Parameter	Cat 1 OD	Cat 1 OS	Cat 2 OD	Cat 2 OS
Zernike coefficients, µm				
C_3, astigmatism at 45°	−0.089 ± 0.086	0.259 ± 0.109	0.221 ± 0.053	0.043 ± 0.093
C_4, defocus	0.087 ± 0.160	0.091 ± 0.061	0.013 ± 0.051	−0.091 ± 0.059
C_5, astigmatism at 0° or 90°	0.022 ± 0.130	−0.171 ± 0.070	−0.004 ± 0.082	−0.196 ± 0.067
HORMS, µm	0.225 ± 0.053	0.269 ± 0.110	0.214 ± 0.031	0.227 ± 0.028
Refractive power, D				
Defocus	0.3 ± 0.5	0.3 ± 0.2	0.0 ± 0.2	−0.3 ± 0.2
Cylinder	−0.7 ± 0.3	−1.4 ± 0.5	−1.0 ± 0.2	−1.0 ± 0.3
Thickness, µm				
Epithelial	59 ± 3	57 ± 3	57 ± 5	56 ± 5
Stromal	500 ± 3	501 ± 3	556 ± 9	567 ± 5
Radius of curvature, mm				
Tear film-epithelium	8.1 ± 0.2	8.18 ± 0.09	8.8 ± 0.1	8.9 ± 0.2
Epithelium-stroma	8.0 ± 0.2	7.9 ± 0.2	8.6 ± 0.2	8.9 ± 0.2
Stroma-endothelium	7.5 ± 0.2	7.0 ± 0.1	7.9 ± 0.2	8.2 ± 0.4

The values are given as mean ± SD.

Investigative Ophthalmology & Visual Science

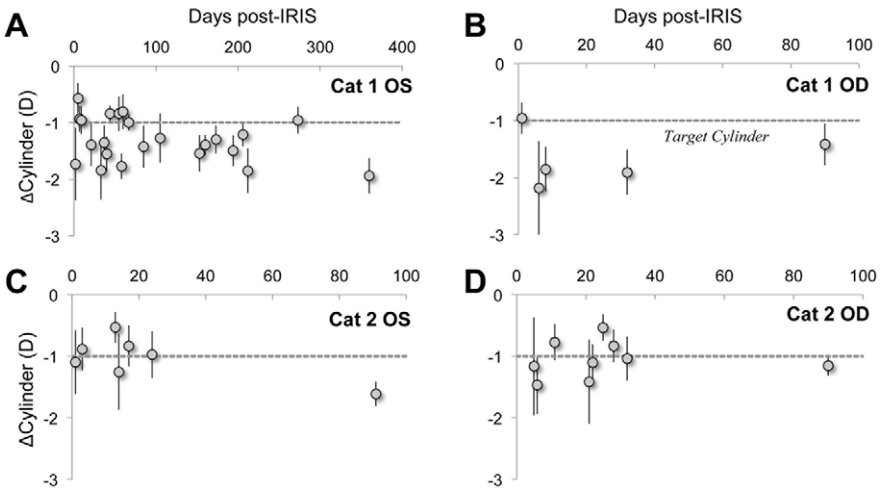

Figure 5. The effect of Blue-IRIS on cylinder expressed as change from baseline. The difference from pre-IRIS cylinder induced by Blue-IRIS in diopters is shown as a function of days post-IRIS. In all cases, the data were collected over a 3-mm-diameter region centered on the approximately 2.5×2.5 mm^2 Blue-IRIS–inscribed pattern, and the *gray, dashed line* indicates the target cylinder induced by Blue-IRIS. (**A**) IRIS-induced cylinder for Cat 1 OS, which had been tracked for 12 months at the time of this report. (**B**) IRIS-induced cylinder for Cat 1 OD. This eye had been tracked for 3 months at the time of this report. (**C**) IRIS-induced cylinder for Cat 2 OS, also tracked for 3 months at the time of this report. (**D**) IRIS-induced cylinder for Cat 2 OD, tracked for 3 months at the time of this report. In spite of some point-to-point variability, the average induction achieved the intended magnitude and sign of cylinder change. *Error bars* represent SDs.

total applanation time to 25 to 45 minutes per eye. Whether long applanation durations contributed to unintended wavefront changes remains to be determined. We are currently working to decrease this time to within 10 minutes, with our final goal being within 3 minutes.

Last, the induced defocus may have originated because Blue-IRIS caused a localized, biomechanical change in the stromal collagen matrix, akin to that observed after PRK or LASIK.[34,35] In these traditional laser refractive procedures, flap cutting severs many of the collagen fibers that span the cornea, changing their tension and creating a slight flattening of the central anterior cornea and peripheral steepening, leading to a hyperopic shift in defocus and an increase in spherical aberration.[16] Given that the change in defocus observed within the small writing area following IRIS was hyperopic, with an accompanying increase in positive spherical aberration, it is conceivable that the Blue-IRIS procedure may have locally weakened the stromal collagen matrix. However, for all three corneal interfaces examined in each eye, OCT revealed no significant changes in the anterior or posterior curvature or discontinuities in any of the interfaces that could have suggested a sustained, localized change in curvature over the IRIS pattern. Regardless, Blue-IRIS has the potential to correct for lower- and higher-order aberrations, which would allow for the implementation of nomograms,[36] or other preemptive measures, to minimize unintended biomechanical changes produced by inscribing a refractive correction.

Finally, it is noteworthy that although the Blue-IRIS patterns were inscribed eccentric to the pupil center, coma induction was minimal. This is likely because the wavefront aberrations were analyzed over a 3-mm-diameter region centered on the IRIS pattern rather than the pupil.[20,22]

Table 2. Mean 1-Month Post-IRIS Data for Each Eye, Expressed as Difference From Pre-IRIS Values for Second-Order Zernike Coefficients ($j = 3$–5), HORMS, Refractive Power, and Mean Post-IRIS Structural Parameters

Parameter	Cat 1 OD	Cat 1 OS	Cat 2 OD	Cat 2 OS
ΔZernike coefficients, μm				
ΔC_3, astigmatism at 45°	−0.007 ± 0.092	−0.194 ± 0.128	0.205 ± 0.076	−0.198 ± 0.100
ΔC_4, defocus	−0.564 ± 0.138	−0.415 ± 0.110	−0.562 ± 0.056	−1.215 ± 0.114
ΔC_5, astigmatism at 0° or 90°	−0.426 ± 0.098	0.363 ± 0.095	0.107 ± 0.069	0.019 ± 0.093
ΔHORMS, μm	0.307 ± 0.045	0.282 ± 0.065	0.251 ± 0.041	0.416 ± 0.031
ΔRefractive power, D				
ΔDefocus	−1.7 ± 0.4	−1.3 ± 0.3	−1.7 ± 0.2	−3.7 ± 0.3
ΔCylinder	−1.9 ± 0.4	−1.8 ± 0.5	−1.0 ± 0.4	−1.0 ± 0.4
Thickness, μm				
Epithelial	67 ± 3	42 ± 3	61 ± 7	62 ± 4
Stromal	503 ± 2	474 ± 3	546 ± 8	551 ± 6
Radius of curvature, mm				
Tear film-epithelium	8.7 ± 0.2	8.8 ± 0.3	8.8 ± 0.2	8.5 ± 0.2
Epithelium-stroma	8.6 ± 0.1	8.6 ± 0.2	8.8 ± 0.3	8.6 ± 0.2
Stroma-endothelium	7.8 ± 0.2	8.1 ± 0.2	7.8 ± 0.2	7.6 ± 0.2

The values are given as mean ± SD.

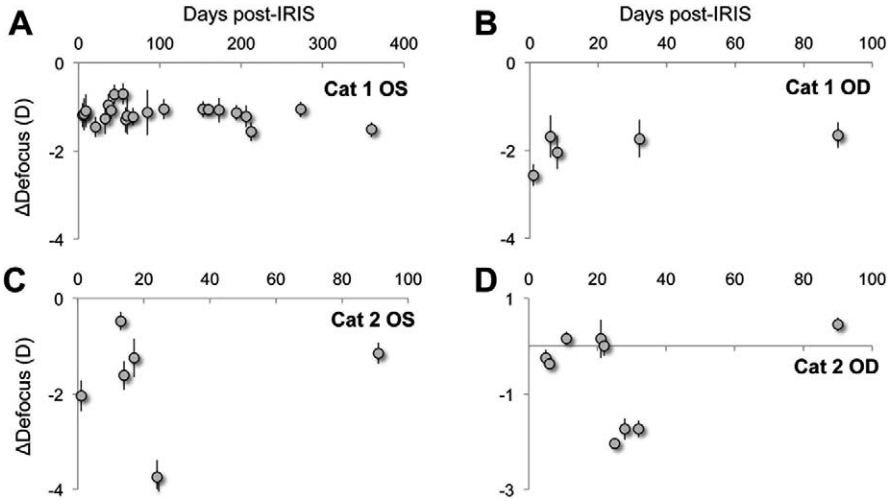

Figure 6. The effect of Blue-IRIS on defocus expressed as change from baseline. Plots of the magnitude of difference from pre-IRIS defocus in diopters induced by Blue-IRIS as a function of days post-IRIS. The data were collected over a 3-mm-diameter measurement aperture centered on the approximately 2.5 mm by 2.5 mm^2 Blue-IRIS pattern. (**A**) The induced defocus in Cat 1 OS. (**B**) The induced defocus in Cat 1 OD. (**C**) The induced defocus in Cat 2 OS. (**D**) The induced defocus in Cat 2 OD. *Error bars* represent SDs.

Blue-IRIS Does Not Increase the Thickness of Different Cornea Layers

The discovery that Blue-IRIS did not increase the thickness of the different corneal layers at the 1-month time-point suggests that it did not cause lingering damage to the corneal endothelium or epithelium that would lead to edema. However, earlier time-points must be examined in the future to verify that no damage was indeed done, as the endothelium may have healed before we took our measurements.[37]

Although not the primary investigation of the present experiment, we do not anticipate Blue-IRIS causing overt damage to the cornea or other elements of the eye. The two-photon nature of the Blue-IRIS allows it to induce refractive changes in the cornea while using laser powers below the ablation threshold for the cornea. This eliminates the overt damage caused by the cutting and ablating typically required in LASIK and PRK. In addition, Blue-IRIS works by focusing laser pulses into the corneal stroma through the epithelium, thereby eliminating the need to debride the epithelium.

Photodamage to the epithelium, endothelium, or retina is also unlikely with Blue-IRIS. Because of the high NA objective used to deliver the femtosecond pulses into the stroma, the laser beam rapidly becomes defocused above and below the focal point. Therefore, the optical power delivered to the epithelial and endothelial layers is spread over a large area. This yields a low irradiance at the epithelium, endothelium, and on the retina.[38]

Temporal Stability of Blue-IRIS–Induced Changes

Blue-IRIS was found to induce a large, stable change in the native refractive state of the cornea over the region in which the IRIS pattern was inscribed. This change was stable for the

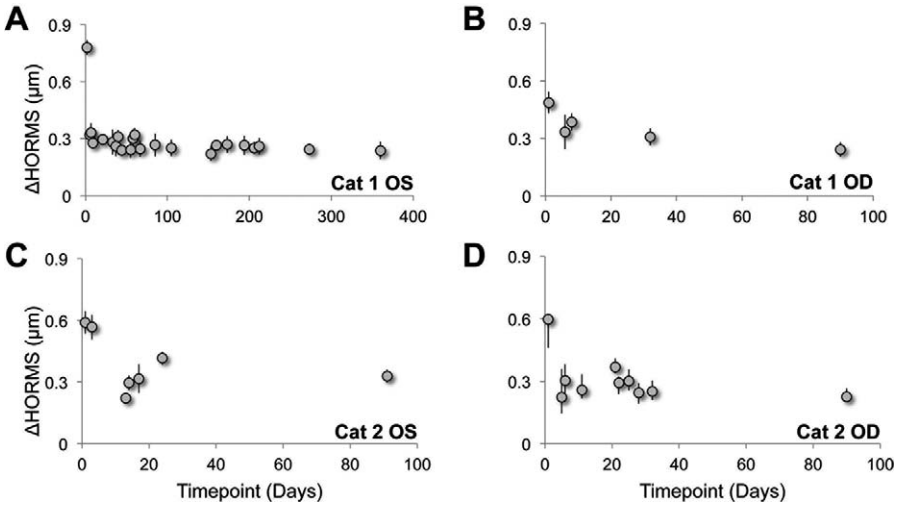

Figure 7. The effect of Blue-IRIS on HORMS expressed as change from baseline. Plots of HORMS ($j = 6$–20) in microns induced by Blue-IRIS as a function of days post-IRIS over a 3-mm-diameter measurement aperture centered on the approximately 2.5 × 2.5 mm^2 Blue-IRIS pattern. The HORMS was calculated from difference from pre-IRIS data. (**A**) The induced HORMS in Cat 1 OS. (**B**) The induced HORMS in Cat 1 OD. (**C**) The induced HORMS in Cat 2 OS. (**D**) The induced HORMS in Cat 2 OD. After some initial fluctuation within the first 1 to 3 days post-IRIS, HORMS tended to converge toward 0.3 μm in all four eyes. *Error bars* represent SDs.

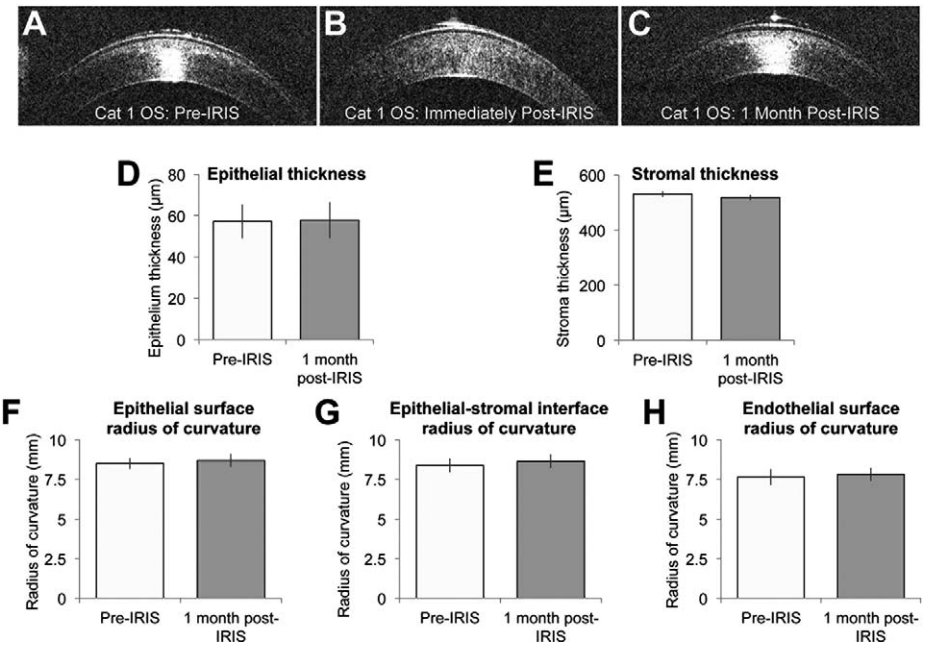

Figure 8. Impact of Blue-IRIS on corneal thickness and curvature. (**A–C**) Optical coherence tomography images of Cat 1 OS at various time-points pre- and post-IRIS. (**D–E**) The mean pre- and 1 month post-IRIS epithelial and stromal thicknesses, respectively, across all four Blue-IRIS–treated eyes. Note the lack of significant change in either measure post-IRIS. (**F–H**) The radii of curvatures of the interfaces between various corneal layers measured pre-IRIS and 1 month post-IRIS. These data also have been averaged across all four eyes in the present study. Note the lack of significant change in any of the curvatures measured. The *error bars* represent the SEM.

duration of the study: approximately 12 months in one eye and 3 months in three more eyes. We will continue to monitor the Blue-IRIS–induced refractive changes in all four eyes reported in this study to further assess the temporal stability of these induced changes beyond the current study period. However, in all four eyes, fluctuations in wavefront aberration magnitude were observed both within and between imaging sessions. Although early fluctuations are potentially a response to the lengthy applanation currently required for Blue-IRIS to be performed in vivo, fluctuations observed at later time-points indicate that another contributing factor is likely to be the small writing area and the difficulty identifying this small pattern within the large pupil area of the cat on individual spot array patterns. These issues, and thus the intermeasurement variability we see here, may be significantly improved once applanation time is reduced and we increase the size of the IRIS pattern to a 6-mm-diameter area.

Table 3. Comparison of Mean Corneal Thicknesses and Radii of Curvature Pre-IRIS and 1 Month Post-IRIS, Averaged Across All Four Eyes

Parameter	Pre-IRIS	1 Month Post-IRIS	*t*-Test
Thickness, μm			
Epithelial	57 ± 4	58 ± 4	$t3 = 0.116$, $P = 0.915$
Stromal	531 ± 6	519 ± 5	$t3 = -2.056$, $P = 0.132$
Radius of curvature, mm			
Tear film-epithelium	8.5 ± 0.2	8.7 ± 0.2	$t3 = 0.784$, $P = 0.490$
Epithelium-stroma	8.4 ± 0.2	8.6 ± 0.2	$t3 = 1.063$, $P = 0.366$
Stroma-endothelium	7.6 ± 0.3	7.8 ± 0.2	$t3 = 0.469$, $P = 0.671$

Paired, two-tailed Student's *t*-tests revealed none of these changes to be statistically significant. The values are given as mean ± SEM.

Conclusions

The present study represents a first in vivo test of a new procedure, Blue-IRIS, which aims to alter the refractive power of a small region of the cornea by locally changing stromal refractive index. Small, lateral GRIN lenses intended to induce approximately a −1 D change in cylinder over the inscribed region of cornea were written noninvasively into anesthetized, living cats. No epithelial debridement, dye doping, flap cutting, or other disruption of the cornea was required. We used wavefront sensing to show that these refractive structures induced an amount of cylinder greater than or equal to the intended change, and that the change was stable for the duration of the study, up to 12 months at the time of writing of this report. Optical coherence tomography imaging showed that the induced optical change was not associated with significant alterations in either corneal thickness or curvature. However, hyperopic defocus and positive spherical aberration were also, unexpectedly, induced by Blue-IRIS. Modifications to the design of the Blue-IRIS treatment could potentially compensate for these aberrations. Future experiments also will characterize the biological consequences of IRIS in the cornea and, more generally, in the eye, with particular attention to potential toxicity of this procedure. Finally, we will continue to investigate the exact mechanism by which IRIS alters the RI of the corneal stroma.

Acknowledgments

The authors thank Christine Callan for excellent veterinary and technical support during cat experiments, Len Zheleznyak and Geunyoung Yoon for the custom-built wavefront sensor, and

Nicholas Brown for his programming contributions. The authors have no proprietary interest in any devices used in this study.

Supported by an unrestricted grant to the University of Rochester's Department of Ophthalmology from the Research to Prevent Blindness Foundation, by the National Institutes of Health (R01 EY015836 [KRH]; Core Grant P30 EY01319F to the Center for Visual Science; Center for Visual Science Training Grant Fellowship T32 EY007125 [DES]), by a grant from Bausch & Lomb, Inc., with matching funds from the University of Rochester's Center for Emerging and Innovative Sciences, and Empire State Development's Division of Science, Technology, and Innovation-designated Center for Advanced Technology. KRH is a Lew R. Wasserman Merit Award recipient.

Disclosure: **D.E. Savage**, None; **D.R. Brooks**, None; **M. DeMagistris**, None; **L. Xu**, None; **S. MacRae**, None; **J.D. Ellis**, None; **W.H. Knox**, None; **K.R. Huxlin**, None

References

1. Kohnen T, Koch DD. *Cataract and Refractive Surgery: With 37 Tables*. Heidelberg, Germany: Physica-Verlag; 2006.
2. Dai G. *Wavefront Optics for Vision Correction*. Bellingham, WA: SPIE Press; 2008.
3. Ding L, Knox WH, Bühren J, Nagy LJ, Huxlin KR. Intratissue refractive index shaping (IRIS) of the cornea and lens using a low-pulse-energy femtosecond laser oscillator. *Invest Ophthalmol Vis Sci*. 2008;49:5332–5339.
4. Nagy LJ, Ding L, Xu L, Knox WH, Huxlin KR. Potentiation of femtosecond laser intratissue refractive index shaping (IRIS) in the living cornea with sodium fluorescein. *Invest Ophthalmol Vis Sci*. 2010;51:850–856.
5. Ding L, Blackwell R, Kunzler JF, Knox WH. Large refractive index change in silicone-based and non-silicone-based hydrogel polymers induced by femtosecond laser micro-machining. *Opt Express*. 2006;14:11901–11909.
6. Ding L, Blackwell RI, Künzler JF, Knox WH. Femtosecond laser micromachining of waveguides in silicone-based hydrogel polymers. *Appl Opt*. 2008;47:3100–3108.
7. Ding L, Cancado LG, Novotny L, et al. Micro-Raman spectroscopy of refractive index microstructures in silicone-based hydrogel polymers created by high-repetition-rate femtosecond laser micromachining. *J Opt Soc Am B*. 2009; 26:595–602.
8. Xu L, Knox WH, Huxlin KR. Exogenous and endogenous two-photon absorption for Intra-tissue Refractive Index Shaping (IRIS) in live corneal tissue [Invited]. *Opt Mater Express*. 2011; 1:1159–1164.
9. Ding L, Nagy LJ, Lisen X, et al. Enhancement of intra-tissue refractive index shaping (IRIS) of the cornea by two-photon absorption. Paper presented at: Conference on Lasers and Electro-Optics; May 31–June 5, 2009; Baltimore, MD.
10. Xu L, Huxlin KR, DeMagistris M, Wang N, Ding L, Knox WH. Non-invasive Blue Intra-tissue Refractive Index Shaping (IRIS) in Living, Excised Cornea. *Frontiers in Optics 2010/Laser Science XXVI*. Rochester, NY; Optical Society of America; 2010:PDPA11.
11. Xu L, Knox WH, DeMagistris M, Wang N, Huxlin KR. Noninvasive intratissue refractive index shaping (IRIS) of the cornea with blue femtosecond laser light. *Invest Ophthalmol Vis Sci*. 2011;52:8148–8155.
12. Noack J, Vogel A. Laser-induced plasma formation in water at nanosecond to femtosecond time scales: calculation of thresholds, absorption coefficients, and energy density. *IEEE J Quantum Electron*. 1999;35:1156–1167.
13. Vogel A, Noack J. Numerical simulations of optical breakdown for cellular surgery at nanosecond to femtosecond time scales. In: Farkas DL, Leif RC, eds. *Volume 4260: Optical Diagnostics of Living Cells IV*. San Jose, CA:SPIE; 2001:83. doi:10.1117/12.426762.
14. Vogel A, Noack J, Hüttman G, Paltauf G. Mechanisms of femtosecond laser nanosurgery of cells and tissues. *Appl Phys B*. 2005;81:1015–1047.
15. Huxlin KR, Yoon G, Nagy L, Porter J, Williams D. Monochromatic ocular wavefront aberrations in the awake-behaving cat. *Vision Res*. 2004;44:2159–2169.
16. Nagy LJ, MacRae S, Yoon G, Cox I, Huxlin KR. Photorefractive keratectomy in the cat eye: biological and optical outcomes. *J Cataract Refract Surg*. 2007;33:1051–1064.
17. Gilger B, Wright J, Whitley R, McLaughlin S. Corneal thickness measured by ultrasonic pachymetry in cats. *Am J Vet Res*. 1993;54:228–230.
18. Huxlin KR, Yoon G, Nagy L, Porter J, Williams D. Monochromatic ocular wavefront aberrations in the awake-behaving cat. *Vision Res*. 2004;44:2159–2169.
19. Huxlin KR, Hindman HB, Jeon K, et al. Topical rosiglitazone is an effective anti-scarring agent in the cornea. *PLoS One*. 2013; 8:e70785.
20. Bühren J, Yoon G, MacRae S, Huxlin K. Contribution of optical zone decentration and pupil dilation on the change of optical quality after myopic photorefractive keratectomy in a cat model. *J Refract Surg*. 2010;26:183.
21. Bühren J, Nagy L, Swanton JN, et al. Optical effects of anti-TGFβ treatment after photorefractive keratectomy in a cat model. *Invest Ophthalmol Vis Sci*. 2009;50:634–643.
22. Bühren J, Yoon G, Kenner S, MacRae S, Huxlin K. The effect of optical zone decentration on lower- and higher-order aberrations after photorefractive keratectomy in a cat model. *Invest Ophthalmol Vis Sci*. 2007;48:5806–5814.
23. Thibos LN, Applegate RA, Schwiegerling JT, Webb R. Standards for reporting the optical aberrations of eyes. *J Refract Surg*. 2002;18:S652–S660.
24. Guirao A, Williams DR. A method to predict refractive errors from wave aberration data. *Optom Vis Sci*. 2003;80:36–42.
25. Thibos LN, Hong X, Bradley A, Applegate RA. Accuracy and precision of objective refraction from wavefront aberrations. *J Vis*. 2004;(4):329–351.
26. Wang J, Fonn D, Simpson TL. Topographical thickness of the epithelium and total cornea after hydrogel and PMMA contact lens wear with eye closure. *Invest Ophthalmol Vis Sci*. 2003; 44:1070–1074.
27. Wang J, Fonn D, Simpson TL, Jones L. The measurement of corneal epithelial thickness in response to hypoxia using optical coherence tomography. *Am J Ophthalmol*. 2002;133: 315–319.
28. Wang J, Fonn D, Simpson TL, Jones L. Relation between optical coherence tomography and optical pachymetry measurements of corneal swelling induced by hypoxia. *Am J Ophthalmol*. 2002;134:93–98.
29. Wang J, Simpson TL, Fonn D. Objective measurements of corneal light-backscatter during corneal swelling, by optical coherence tomography. *Invest Ophthalmol Vis Sci*. 2004;45: 3493–3498.
30. Wang J, Thomas J, Cox I. Corneal light backscatter measured by optical coherence tomography after LASIK. *J Refract Surg*. 2006;22:604–610.
31. Wang J, Thomas J, Cox I, Rollins A. Noncontact measurements of central corneal epithelial and flap thickness after laser in situ keratomileusis. *Invest Ophthalmol Vis Sci*. 2004;45:1812–1816.
32. Radhakrishnan S, Rollins AM, Roth JE, et al. Real-time optical coherence tomography of the anterior segment at 1310 nm. *Arch Ophthalmol*. 2001;119:1179–1185.
33. Xu L, Knox WH. Lateral gradient index microlenses written in ophthalmic hydrogel polymers by femtosecond laser micromachining. *Opt Mater Express*. 2011;1:1416–1424.

34. Roberts C. The cornea is not a piece of plastic. *J Refract Surg*. 2000;16:407–413.
35. Dupps WJ Jr, Wilson SE. Biomechanics and wound healing in the cornea. *Exp Eye Res*. 2006;83:709–720.
36. Subbaram MV, MacRae SM. Customized LASIK treatment for myopia based on preoperative manifest refraction and higher order aberrometry: the Rochester nomogram. *J Refract Surg*. 2007;23:435–441.
37. Lundberg B, Jonsson M, Behndig A. Postoperative corneal swelling correlates strongly to corneal endothelial cell loss after phacoemulsification cataract surgery. *Am J Ophthalmol*. 2005;139:1035–1041.
38. Xu L. Femtosecond laser processing of ophthalmic materials and ocular tissues: a novel approach for non-invasive vision correction. Rochester, NY: University of Rochester; 2013:344.

Investigative Ophthalmology & Visual Science